Global reconstruction: application to biological data and secure communication

Natalia B. Janson[1], Alexey N. Pavlov[2], Vadim S. Anishchenko[2]
[1] *Physics Department, Lancaster University, Lancaster LA1 4YB, UK*
[2] *Physics Department, Saratov State University, Astrakhanskya str. 83, 410026 Saratov, Russia*
()

We discuss two applications of global reconstruction approach. The *first* one is creation of empirical models from one-dimensional time series resulting from medical and biological experiments. Namely, we apply the approach to signals from isolated frog heart (IFH) and from human electrocardiogramme (ECG) in order to obtain systems of ordinary differential equations and discrete maps with solutions similar to the signals measured. We try to solve the problem using standard techniques for phase portrait reconstruction and present the results which, though not providing good quantitative description, seem to preserve qualitative information about the structure of the associated attractor quite well. We discuss the difficulties when building models for highly inhomogeneous signals like ECG which are combinations of segments with fast motion and those with almost no motion. We suggest to overcome the problem using a special method for phase portrait reconstruction which results in the simplest form of the evolution equations.

Second, we propose to exploit the global reconstruction approach for the purposes of secure communication with several independent information channels.

I. GLOBAL RECONSTRUCTION: MODELLING BIOLOGICAL DATA

A. Description of the algorithms

In this Section we make a black box assumption about the system under study. The designations used in this Section of the paper are enlisted in Table 1. A detailed description of a typical reconstruction procedure with relevant references is given in Chapter 1 of this book. Here, we briefly remind the reader about the stages of reconstruction process. The first stage includes reconstruction of the phase portrait of the system. In Section I.B. we use two popular methods, namely, delay embedding and method of successive derivatives. In Section I.C. we also propose the use of the successive integration to embed substantially inhomogeneous signals like human electrocardiogramme (ECG). This step also involves estimation of embedding dimension N.

$a(t)$	experimental signal
x_j	reconstructed coordinates
j	number of reconstructed coordinate, j=1,...,N
N	embedding dimension
θ	embedding delay
τ_0	first zero of autocorrelation function
τ_{min}	first minimum of autocorrelation function
L	number of sample points selected for least squares fitting
ν	order of polynomial
$C_{j,l_1 l_2 \ldots l_N}$	coefficients in the right-hand part of j -th reconstructed equation
D	intensity of noise added to reconstructed equations

Table 1. Designations for reconstruction parameters used in this chapter.

At the second stage, we look for a dynamical systems in the form of an N-dimensional discrete map

$$\begin{aligned} x_{1,k+1} &= f_1(x_{1,k}, x_{2,k}, \ldots, x_{N,k}), \\ x_{2,k+1} &= f_2(x_{1,k}, x_{2,k}, \ldots, x_{N,k}), \\ &\ldots \\ x_{N,k+1} &= f_N(x_{1,k}, x_{2,k}, \ldots, x_{N,k}), \end{aligned} \tag{1}$$

or a system of N ordinary differential equations (ODE)

$$\begin{aligned} dx_1/dt &= f_1(x_1, x_2, \ldots, x_N), \\ dx_2/dt &= f_2(x_1, x_2, \ldots, x_N), \\ &\ldots \\ dx_N/dt &= f_N(x_1, x_2, \ldots, x_N). \end{aligned} \tag{2}$$

Here, $x_{j,k}$ or x_j are phase coordinates. In Eq. (1) k is the number of iteration (equivalent of time). f_j are some nonlinear functions that are here presented as polynomials of the order ν:

$$f_j(x) = \sum_{l_1 l_2 \ldots l_N = 0}^{\nu} C_{j,l_1 l_2 \ldots l_N} \prod_{k=1}^{N} x_k^{l_k}, \quad \sum_{k=1}^{N} l_k \leq \nu.$$

$C_{j,l_1 l_2 \ldots l_N}$ are the coefficients sought. For such a polynomial representation of right-hand parts of the model, the number N_c of coefficients in one equation is:

$$N_c = \frac{(N+\nu)!}{N!\nu!} \tag{3}$$

Note, that when the phase coordinates are reconstructed by means of successive differentiation or integration of the original data, and then possibly rescaled to fit into the interval $[0:1]$, the ODEs sought as a result of fitting procedure might become (but not always) of the following form:

$$\begin{aligned} dx_1/dt &= C_{1,010\ldots} x_2, \\ dx_2/dt &= C_{2,001,\ldots} x_3, \\ &\ldots \\ dx_N/dt &= f(x_1, x_2, \ldots, x_N), \end{aligned} \tag{4}$$

where the non-unity coefficients in all equations except the last one appear due to possible rescaling of the data. If no rescaling was done, these coefficients are equal to 1.

To find the coefficients, a least squares method was applied. L datapoints were taken from the whole dataset while moving along it with some fixed step. We chose ν, starting with the smallest 2, performed fitting of the coefficients and validated the model. If the model was unsuccessful, we repeated the procedure by varying the number of sample datapoints L and ν, until a successful model was found.

To validate the model, we visually compared its solutions (signals) and phase portraits, and also the statistical properties of the solutions with the original ones. It was crucial that the reconstructed system possessed an attractor of required shape, and the trajectory did not go to infinity in a reasonably large vicinity of it. We also checked if the model was robust towards slight variations of control parameters. Only a robust model possessing the required attractor with reasonably large basin of attraction, whose solutions had the similar shape and statistical properties was considered successful.

Sometimes, to make a more thorough comparison of the experimental data and the obtained model, we add noise terms to the obtained equations. Namely, to all N right-hand parts f_j we add stochastic terms in the form $D\xi_j(k)$ for maps (1) or $D\xi_j(t)$ for ODEs (2). Here, ξ_j are independent sources of Gaussian white noise with zero average and unity variance, and D is noise intensity.

B. Standard reconstruction techniques applied to biological data

Isolated frog heart. For a very simple example of a signal $a(t)$ of biological origin, consider measurements from an isolated heart of a frog. A heart was taken out from a frog and put into the special solution where it continued to contract. A metal hook was stuck into the heart surface. As heart contracted, the points on surface moved correspondingly, and the hook moved together with the point it was stuck into. The position of the hook was followed, digitized and fed into the computer. Sampling rate was 60 Hz, resolution 8 bits, and the duration of recording 136 sec.

The results on reconstruction of models from signals of isolated frog heart were in part published in [2,3].

The oscillations of a heart of a frog isolated from the rest of the organism and thus experiencing no influence usual for a living system are very close to periodic, contaminated by noise. The average frequency of a typical frog's heart contraction was about 0.6 Hz. A typical signal measured from such a heart, which we will further denote IFH for brevity, is shown in Fig. I.1(a). Its statistical characteristics are given in Fig. I.2: Fourier power spectrum in (a) and autocorrelation function in (b). All the features of the functions shown support the inference about nearly periodicity of oscillations: sharp spectral peaks at the positions being multiples of the main peak at about 0.6 Hz, and slowly decreasing autocorrelation function.

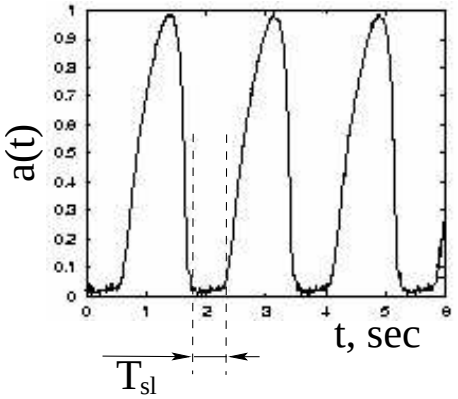

Fig. I.1. A typical signal measured from isolated frog heart (IFH).

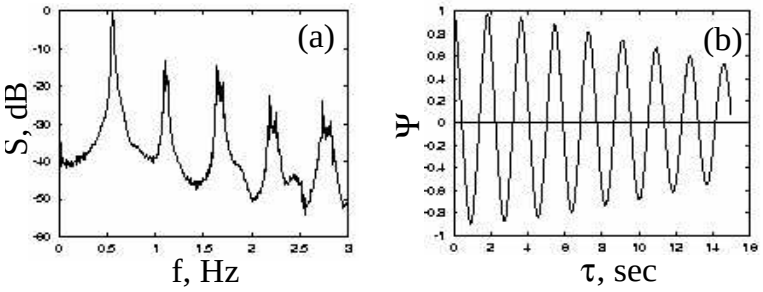

Fig. I.2. (a) Fourier power spectrum $S(f)$, (b) autocorrelation function $\Psi(\tau)$ of IFH signal.

As a first step, we need to reconstruct the phase portrait of a dynamical system which supposedly underlies the observed motion. Since oscillations seem to be periodic ones affected by noise, the corresponding attractor should be a limit cycle. According to Takens theorem [1], the dimension $N = 3$ of the system phase space is enough to embed any limit cycle, and in some cases $N = 2$ might be enough.

To reconstruct a phase portrait, we choose delay embedding for which we need to find an optimal time delay θ. We have tried various time delays, also taking into account popular criteria like the first zero τ_0 and

the first minimum τ_{min} of autocorrelation function $\Psi(\tau)$. The use of the latter time delays resulted in phase portraits whose projections to the plane are shown in Fig. I.3(a,b). With this, the use of a small θ roughly equal to 1/20th of the basic period of oscillations, results in a phase protrait of rather simple form without self-intersections on the plane (Fig. I.3(c)). It is obvious that due to the self-intersections in Fig. I.3(a) and a cusp in Fig. I.3(b), embedding dimension

$N = 2$ is not sufficient for these phase portraits, while the one in Fig. I.3(c) fits well onto the phase plane with $N = 2$. Since we are interested in a dynamical system of the simplest form, we prefer a smaller-dimensional system to be found and thus apply global reconstruction techniques to the phase portrait presented in Fig. I.3(c).

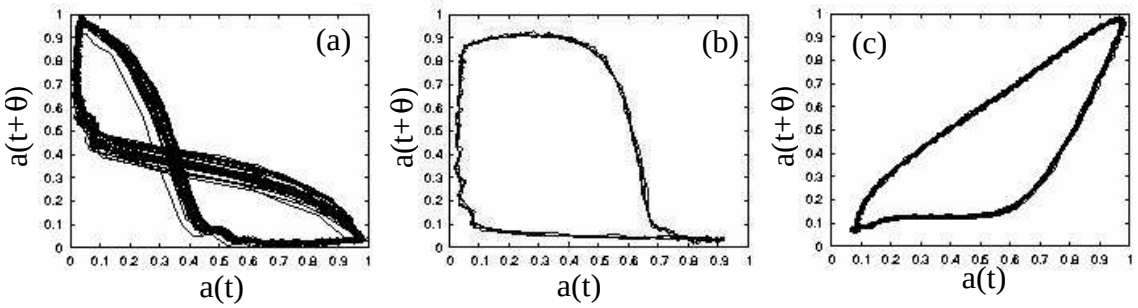

Fig. I.3. Delay embedding of IFH with different values of time delay θ: (a) $\theta = \tau_0$ (b) $\theta = \tau_{min}$ (c) $\theta = 0.08(3)sec.$

We first seek for a model in the form of a discrete map Eq. (1). After some experimentation, we pick $L = 300$ points for the least squares procedure that are uniformly spread along the data set available. Suitable 2-dimensional maps were obtained for the order of polynomial $\nu = 4$. The phase portrait and temporal behavior of a coordinate x_1 are shown in Fig. I.4(a) and (b), respectively. One can compare them with the phase portrait in Fig. I.3(c) and the initial signal in Fig. I.1(a). The statistical characteristics for the given solution were computed from the dataset of the same length as the original one and are presented in Fig. I.5. The designations are the same as in Fig. I.2. The equations without noise produce a periodic attractor with the shape similar to the original phase portrait and period close to the one of the original signal. However, the spectral peaks of the experimental signal $a(t)$ are somewhat wider than in the reconstructed data, and the autocorrelation function $\Psi(\tau)$ slowly decreases. This might be due to the inevitable presence of noise in the original data. To simulate a situation closer to reality, we add noise with intensity $D = 10^{-2}$ to the obtained equations, find the solution and compare its statistical properties with those of the original signal. The solution of system with noise is illustrated in Fig. I.6 and its statistical characteristics in Fig. I.7. It seems that the reconstructed system with noise provides a better description of the real situation.

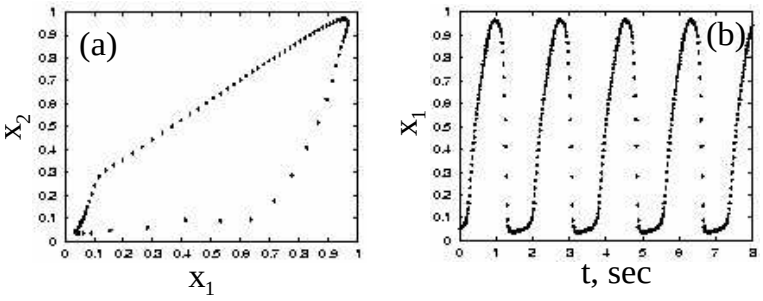

Fig. I.4. Solution of map reconstructed from IFH: (a) phase portrait (b) coordinate x_1 vs discrete time.

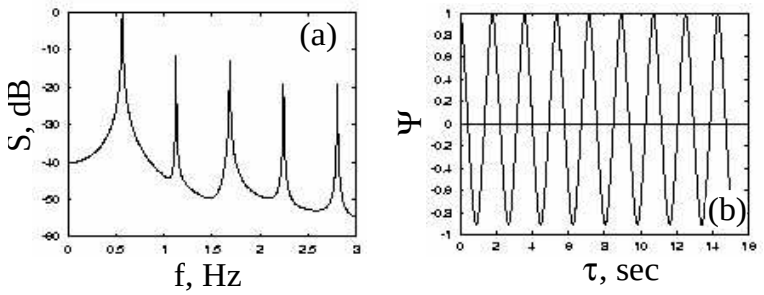

Fig. I.5. (a) Fourier power spectrum S(f); (b) autocorrelation function $\Psi(\tau)$ of the solution of model map reconstructed from IFH.

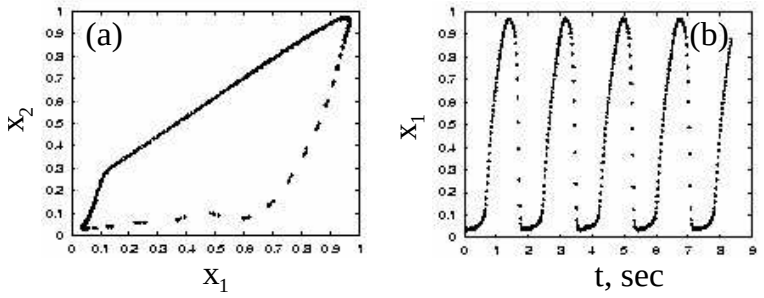

Fig.I.6. Solution of map reconstructed from IFH with added noise of intensity $D = 10^{-2}$: (a) phase portrait (b) coordinate x_1 vs discrete time.

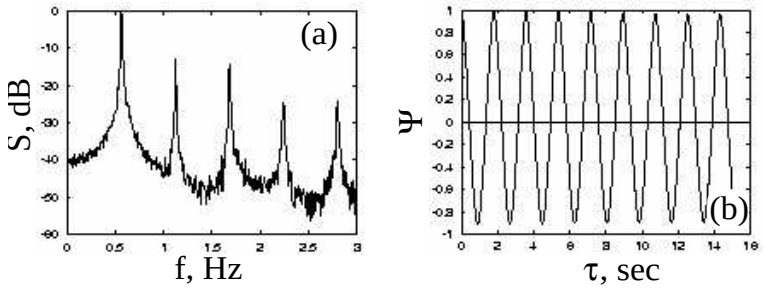

Fig. I.7. (a) Fourier power spectrum S(f); (b) autocorrelation function $\Psi(\tau)$ of the solution of model map reconstructed from IFH with added noise.

Second, we try to reconstruct a system of ODE in the form of Eq. (2) to fit the IFH data. It turned out that $N = 2$ was not enough to obtain a satisfactory model for order of polynomial ν less than 10. We increased N up to 3 and for $\nu = 4$ and $L = 1000$ obtained a satisfactory model whose solution is shown in Fig. I.8 to compare favorably with the original data.

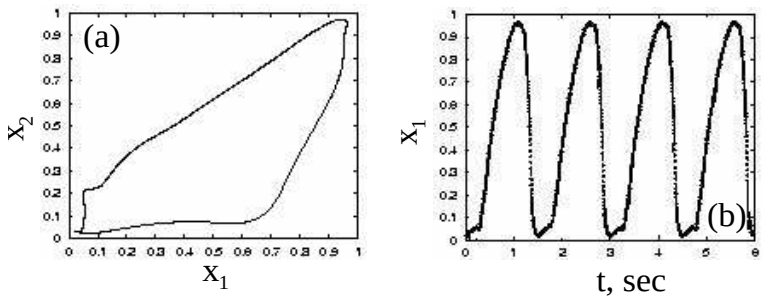

Fig. I.8. Solution of system of three ODEs reconstructed from IFH data: (a) phase portrait (b) coordinate x_1 versus time t.

While dealing with this seemingly easy example of oscillations close to periodic and with rather simple shape, we make the following observation. It was relatively easy to find models that provided a reasonably good description of the original data, and the whole process of reconstruction appeared to be quite robust towards variation of algorithm parameters. However, all models obtained possess two common features: (1) unlike the original signal $a(t)$, their solutions $x_j(t)$ never included segments which were close to horizontal (a horizontal segment is bounded by dashed lines in Fig. I.1(a)), (2) their phase portraits (Figs. I.4(b), 6(b), 8(b)) in the lower left corners are more curvy than the original one in Fig. I.3 (c). We did not succeed in finding a better description for these data by trying reasonably large range of polynomial orders ν and dimensions N. We will discuss the reason for this phenomenon in Section I.C. of this chapter.

Human electrocardiogramme (ECG). This is a signal reflecting electrical activity of human heart [4]. A signal was taken from the II standard lead on the human body, sampled with frequency 200 Hz and digitized with resolution 8 bit, the duration of recording is 180 sec. The results on global reconstruction of ECGs were partly published in [5–9], but here we give more detailed illustrations of reconstruction process and results.

A typical ECG is shown in Fig. I.9 (a), and its statistical characteristics are given in Fig. I.10. Designations are the same as in Figs. I.2, I.5, I.7. Although it might not be obvious from looking at a small sample of the signal in Fig. I.9(a) which contains only three typical periods of ECG, that is, three heart beats, it is now well acknowledged that normally ECG is not periodic [10]. This feature is supported by the Fourier power spectrum (Fig. I.10(a)) which appears to be continuous and contains several smeared peaks at the basic frequencies: the main one at average heart rate f_{ahr}, the second one at the frequency of respiration f_{resp}, the third one at the frequency whose origin is not ambiguously established yet, and is sometimes attributed to parasympathetic system activity f_p. Autocorrelation function (Fig. I.10(b)) decreases rapidly and almost exponentially in the beginning, that testifies to a large degree of disorder in the system.

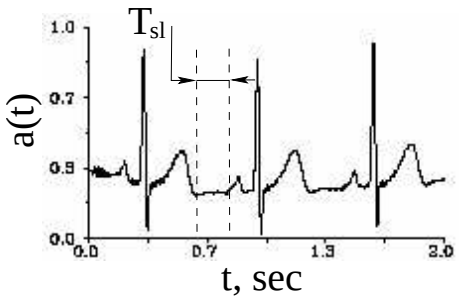

Fig. I. 9. A typical human electrocardiogramme. T_{sl} is the duration of "slow" segment.

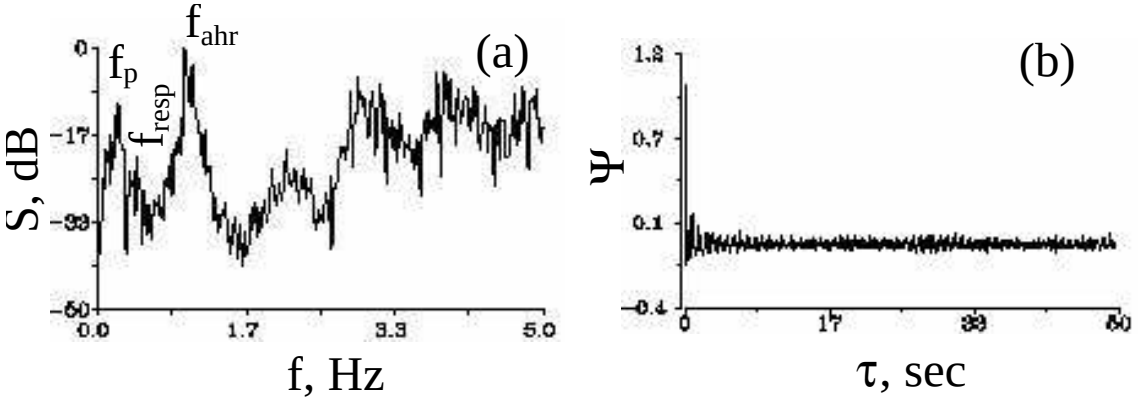

Fig. I.10. (a) Fourier power spectrum S(f); (b) autocorrelation function $\Psi(\tau)$ of a typical human ECG.

Application of standard method for global reconstruction to a phase portrait, reconstructed from ECG by means of *delay embedding* with any value of delay θ, embedding dimension N up to 5, and order of polynomial ν up to 10, did not lead to any successful model.

We then reconstructed phase portrait by successive derivatives, whose projections onto the three phase planes are shown in Fig. I.11 (a,b,c), and the reconstructed phase coordinates in Fig. I.12(a,b,c). We also rescale all the reconstructed coordinates so that each fits into the interval $[0 : 1]$. For $N = 3$, $\nu = 3$, a thorough selection of sample points number L and the step of their sampling over the dataset, allowed one to obtain a model whose phase portrait projected onto different planes is shown in Fig. I.11(d,e,f), and the phase coordinates in Fig. I.12(d,e,f). The coefficients found are given in Table 2.

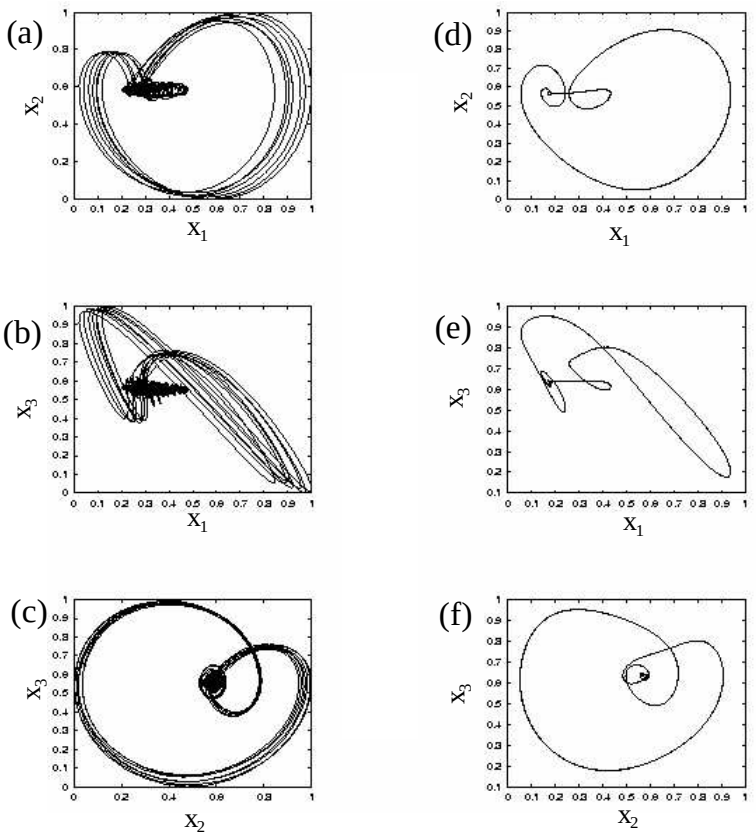

Fig. I.11. Projections of phase portrait: (a), (b), (c) reconstructed from ECG by means of derivatives; (d), (e), (f) of the reconstructed system of three ODEs.

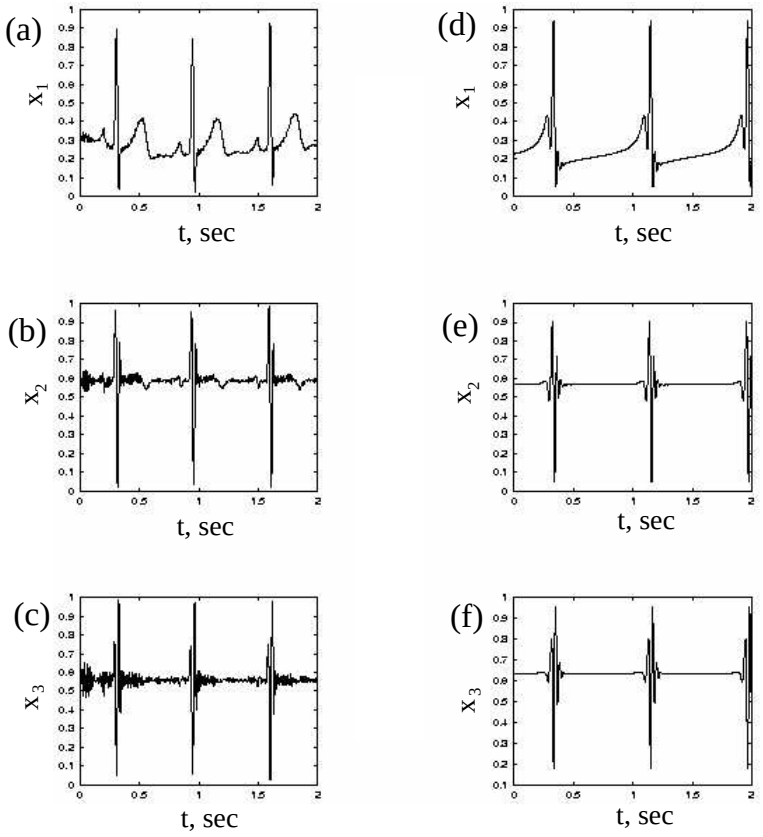

Fig.I.12. Phase coordinates versus time (a), (b), (c) of phase portrait reconstructed from ECG by means of derivatives; (d), (e), (f) of the reconstructed system of three ODEs.

l_1	l_2	l_3	$C_{1,l_1l_2l_3}$	$C_{2,l_1l_2l_3}$	$C_{3,l_1l_2l_3}$
0	0	0	-62.8815605603704	74.82752942560485	3071.083665436582
0	0	1	-87.42192330952132	-408.1605444577854	-8044.035575772645
0	0	2	148.4098020618565	645.0986794252472	7241.059151999466
0	0	3	-71.18814916947224	-244.4656009391038	-2237.791710386605
0	1	0	162.7534113897522	-66.30831825551626	-2698.370510396959
0	1	1	-30.73538735418802	127.2347810104990	4132.591119361165
0	1	2	-14.72974583020030	-96.28985948316979	-1949.402043984592
0	2	0	-35.60776546416798	-56.55029446018383	854.4011163023006
0	2	1	51.12904820744647	112.6292099863897	228.7322718643860
0	3	0	1.932585151134665	-14.78871631683085	-727.2423594608101
1	0	0	-30.07536965229423	-337.4525776296231	-5769.989846188379
1	0	1	84.17628639605554	711.3590104753229	10974.20763003941
1	0	2	-56.92549847251272	-393.0358547306519	-4828.899521920600
1	1	0	9.045568106455534	175.0880927639325	2615.201156634225
1	1	1	-20.75865261431480	-208.2602811584960	-2778.335341888779
1	2	0	2.293211838270821	24.33515899303961	411.8750336509210
2	0	0	9.898513917266278	160.3164864496251	3647.470844441290
2	0	1	-10.98040119221886	-153.1590240864454	-4048.252351004705
2	1	0	-1.088871114278943	-59.26510874155975	-1003.206276979911
3	0	0	0.5386944386575726	-18.83938344983301	-597.5953842340851

Table 2. Coefficients of the model reconstructed from ECG. Original phase portrait was reconstructed by successive differentiation of initial ECG.

l_1	l_2	l_3	$C_{3,l_1l_2l_3}$
0	0	0	-560.0
0	0	1	-180.0
0	0	2	-1.31356
0	0	3	-0.00196
0	1	0	2140.0
0	1	1	-8.3
0	1	2	0.0
0	2	0	230.0
0	2	1	0.0
0	3	0	-230.0
1	0	0	-17700.0
1	0	1	-1240.0
1	0	2	-4.4
1	1	0	-3850.0
1	1	1	90.0
1	2	0	-70.0
2	0	0	-46525.0
2	0	1	-2250.0
2	1	0	-20000.0
3	0	0	33618.0

Table 3. Coefficients of the 3-rd equation of the model reconstructed from ECG. Original phase portrait was reconstructed by successive integration of a periodic signal, artificially created by cutting out a single "beat" of ECG and its repetition.

The first observation is that inspite of the non-periodicity of the original oscillations, the solution of the best reconstructed model is periodic. Second, the shape of a single "beat" in the original ECG and in the solution of the reconstructed system are different in an essential detail: while ECG possesses almost horizontal segments reflecting no motion (Fig. I.9), there are no such horizontal segments in the associated coordinate x_1 of the reconstructed system (compare Figs. I.12(a) and (d)). We will return to the reason for this feature in Section I.C. of this chapter. Third, the obtained model does not preserve the feature of the original reconstructed phase coordinates in that the second coordinate is not already the derivative of the first one. The consequence is that the obtained equations do not have anticipated reduced form Eq. (4), but rather look like Eq. (2).

We now want to make a more thorough validation of the obtained model and study its properties in more detail. There are *several equilibrium states* in the system, but only three of them lie in the vicinity of the attractor shown in Fig. I.11 (d,e,f). Since the obtained system has a complex form, it is difficult to analyze its equilibria analytically and we do this numerically.

The *basin of attraction* of the limit cycle in Fig. I.11 (d,e,f) is about the size of the cycle itself. From initial conditions outside this basin the trajectory goes to infinity.

We then vary the model parameters in order to see whether/ how the *regimes change*. To do so, we need to figure out several parameters out of total $N_c = 60$, whose variation causes qualitative change of regimes, i.e., through bifurcations. By manually changing parameter values, integrating the system and observing the resulting phase portrait, we find a parameter $C_{2,000}$ (underlined in Table 2) whose variation leads to

bifurcations in the system. As this parameter is changed, one observes transitions from the periodic regime in Fig. I.11 (d,e,f) to chaotic, whose phase projection is given in Fig. I.13 (a) and statistical characteristics in Fig. I.13 (b,c). Note, that Fourier power spectrum is continuous for chaotic regime, and autocorrelation function decreases in a manner similar to that of the original ECG (Fig. I.10(a,b)).

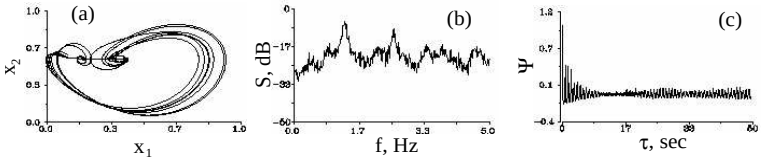

Fig. I.13. (a) phase portrait of the system of three ODEs reconstructed from ECG (model parameters are given in Table 2) in a chaotic regime (to be compared with Figs. I.11 (a) and (d)). (b) Fourier power spectrum S(f) and (b) autocorrelation function $\Psi(\tau)$ of the chaotic regime (to be compared with Figs. I.10(a) and (b)).

In [11], based on observation of the shape of a typical human ECG, a hypothesis was suggested that the motion in the system phase space is close to that resulting from the existence of a homoclinic orbit (loop) to the saddle fixed point in a vicinity of the observed regime. Some numerical evidence for the plausibility of this hypothesis was provided as well. If our model captures some essential qualitative features of ECG dynamics, it should possess a saddle equilibrium and a homoclinic orbit in some parameter vicinity of attractor of our interest. One should note that generally homoclinic loop is a non-robust structure which vanishes under infinitely small variation of control parameters. In our model, we found a saddle equilibrium in the basin of attraction of the limit cycle of interest, and for a certain value of $C_{2,000}$ a homoclinic loop shown in Fig. I.14. Eigenvalues of the saddle fixed point were found to be $s_{1,2} \approx 78 \pm 92i$, $s_3 \approx -45$. A saddle quantity $\sigma = Res_{1,2} + s_3 \approx 33$ is less than zero. According to Shil'nikov's theorem [12], when this loop is destroyed, a chaotic set is formed, not necessarily attracting. This set can become attracting when the existing regime looses its stability.

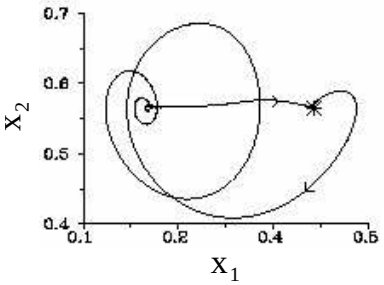

Fig. I.14. Homoclinic orbit to a saddle equilibrium in the system of three ODEs (Table 2).

To summarize, we provided illustration how standard tools for global reconstruction of dynamical systems from experimental data work as applied to real signals of biological origin. It seems that for periodic signals of relatively simple shape one can obtain an approximate model quite easily. However, the presence of segments with very slow motion in datasets lead to problems with reconstructing appropriate models with the same feature.

C. Global reconstruction from substantially inhomogeneous signals

In this section we address the particular problem arising when one attempts to build a global model from an essentially inhomogeneous signal. We call a signal *inhomogeneous* if it consists of segments of very slow motion, i.e. almost horizontal, and segments with fast motion. Two examples of inhomogeneous signals encountered in biology are the signal from a frog heart (Fig. I.1(a)) and a human electrocardiogramme (Fig. I.9(a)).

In Section I.B. we gave examples of best models obtained from these essentially inhomogeneous signals, when two standard methods for phase portrait reconstruction were applied: successive differentiation and delay embedding. A common feature of all such models is that their coordinates related to the original signals become less inhomogeneous (compare Fig. I.1(a) with I.4(a) and I.8(a), and Fig. I.9(a) with I.11(a)). In particular, the "slow" segments become visibly faster, so that the coordinate no longer possesses horizontal segments. This means that although the reconstructed models might describe the original systems qualitatively, they do not provide good quantitative description.

Here, we discuss methods for reconstruction of the phase portrait from an essentially inhomogeneous signal, with respect to the properties of the models which they result in.

Successive derivatives. $\vec{x}(t)$ is reconstructed from the original signal $a(t)$ as follows:

$$\vec{x}(t) = \{a(t), da(t)/dt, \ldots, d^{N-1}a(t)/dt^{N-1}\}. \tag{5}$$

The major attraction of this method is the possibility to obtain a model of a simplified form (4). However, for substantially inhomogeneous signals, successive differentiation will lead to signals which are more and more inhomogeneous. Namely, "slow" segments will further slow down and become closer to horizontal, while "fast" segments will either preserve or increase the velocity of their motion (Fig. I.15). This means that in the reconstructed phase space, there are very small areas where the trajectory spends much time, and large areas where the trajectory goes quickly. Phase portrait reconstructed from an ECG by derivatives in a 3-dimensional phase space is shown in Fig. I.16. An exit from the area with slow motion means an abrupt increase of the absolute phase velocity from almost zero to some finite value. The smaller the "slow" area, the more abrupt the transition. This means that the flow varies quickly in the vicinity of the "slow" area, and one requires quite a large order of polynomial to fit it. At the same time, there are computational restrictions on the maximal polynomial order which one can use effectively.

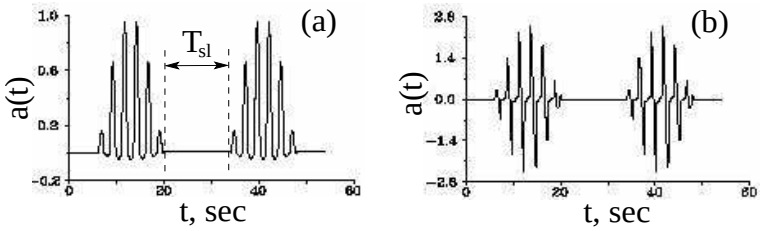

Fig.I.15. (a) An example of inhomogeneous signal and (b) its derivative. T_{sl} is the duration of "slow" segment.

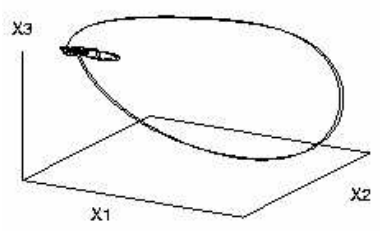

Fig. I.16. Phase portrait reconstructed from ECG by means of derivatives in 3-dimensional phase space.

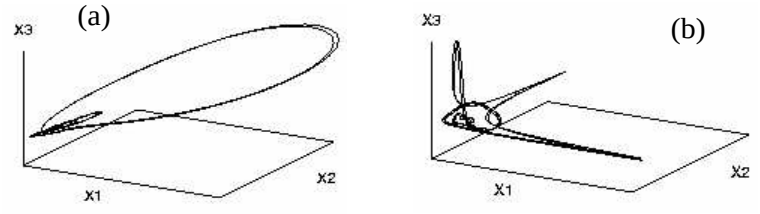

Fig. I.17. Phase portrait reconstructed from ECG by delay embedding in 3-dimensional space (a) θ is much less than, and (b) θ is close to, the duration of "slow" segment T_{sl} in Fig. I.9.

Delay embedding. The seemingly easiest, and thus very popular, method is delay embedding, which gives a reconstructed phase vector $\vec{x}(t)$ as follows:

$$\vec{x}(t) = \{a(t), a(t+\theta), \ldots, a(t+(N-1)\theta)\}. \tag{6}$$

This method results in a model having the form of Eqs. (2), which is more complex than the one that can arise from successive derivatives. However, this method can possibly overcome the problem of "slow" areas arising in the derivatives method. Let θ be an $1/M$-th ($M > 2$) fraction of the average duration of a "slow" segment T_{sl} in original signal (see Fig. I.15(a)). Let $a(t)$ belong to the start of the "slow" segment. Then $a(t+\theta), a(t+2\theta), \ldots, a(t+M\theta)$ are almost equal to $a(t)$. If the embedding dimension N is less than M, this will result in the same problem as that mentioned for derivatives embedding. In Fig. I.17(a) a phase portrait reconstructed from an ECG in 3-dimensional space with small values of θ is shown. To avoid the creation of the region with slow motion, one can either increase N, which is not quite appealing, or increase θ. When θ is increased to the values comparable with T_{sl}, the isolated "slow" area vanishes, so the problem seems to be solved. However, another sort of regions with quick variation of phase velocity appear simultaneously (Fig. I.17(b)), what leads to the same problem with fitting the model.

Integral embedding. To resolve problems caused by differential and delay embeddings of essentially inhomogeneous signals, we propose to use integral embedding for at least several components of reconstructed vector as follows:

$$\vec{x}(t) = \{x_1(t), x_2(t), x_3(t), \ldots\},\ x_1(t) = a(t),\ x_2(t) = \int_0^t x_1(t)dt,\ x_3(t) = \int_0^t x_2(t). \tag{7}$$

For signal $a(t)$ with zero average value, integration acts as the opposite of differentiation, namely, it speeds up "slow" segments and slows down the fast ones. Even when "slow" segments are perfectly horizontal at some non-zero level, the intergal of them changes linearly in time. With this, unlike delay embedding with large enough θ, integration does not create another sort of regions in the phase space with fast variation of phase velocity. At the same time, the reconstructed model contains the equations of simplified form (4) whose number coincides with the number of integrations used.

An essential drawback of this technique is its strong sensitivity to even slightest floating of average level of the dataset $a(t)$. We will not further discuss this problem here, and for illustrations of the workability of this method will use only strictly periodic data.

We will concentrate on the more complex of two examples of essentially inhomogeneous biological signals being human ECG $a(t)$. To test the proposed integration method and to avoid dealing with the floating average level, we cut out a segment of ECG between the two neighboring R peaks and create a signal consisting of many repetitions of this segment. We thus obtain a strictly periodic signal with precisely constant average value, which we then subtract from the dataset. From this artificially created signal $a(t)$ we reconstruct a phase portrait by integral embedding with $N = 3$ as follows:

$$x_3(t) = a(t),\ x_2(t) = \int_0^t x_3(t),\ x_1(t) = \int_0^t x_2(t). \tag{8}$$

The three projections of the phase portrait and the three reconstructed phase coordinates versus time are shown in Fig. I.18. We choose the order of polynomial $\nu = 3$ and fit the equations of the form Eq. (4), with $C_{j,000} = 1$, $j = 1, 2$. The coefficients of the 3-rd equation are given in Table 3.

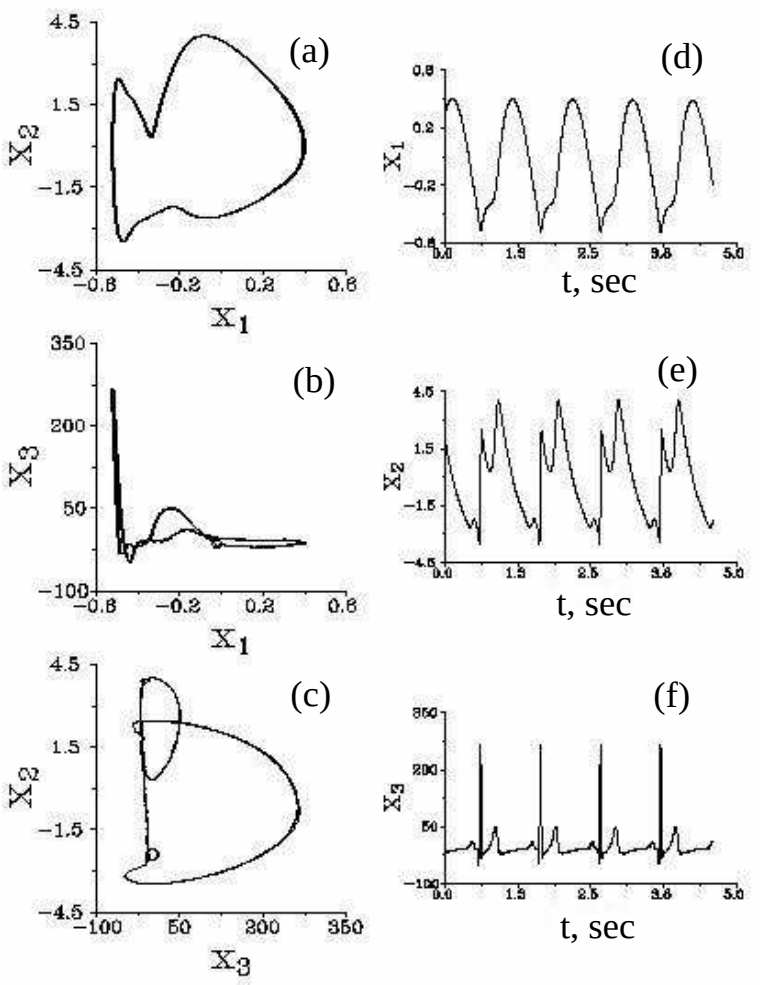

Fig. I.18. (a), (b), (c) Projections of the phase portrait and (d), (e), (f) phase coordinates versus time, reconstructed from ECG by successive integration in 3-dimensional phase space. Details are given in text.

The solution of the reconstructed model is illustrated in Fig. I.19. One can see "slow" segments now present in the coordinate x_3 of the reconstructed model, which is associated with the original ECG.

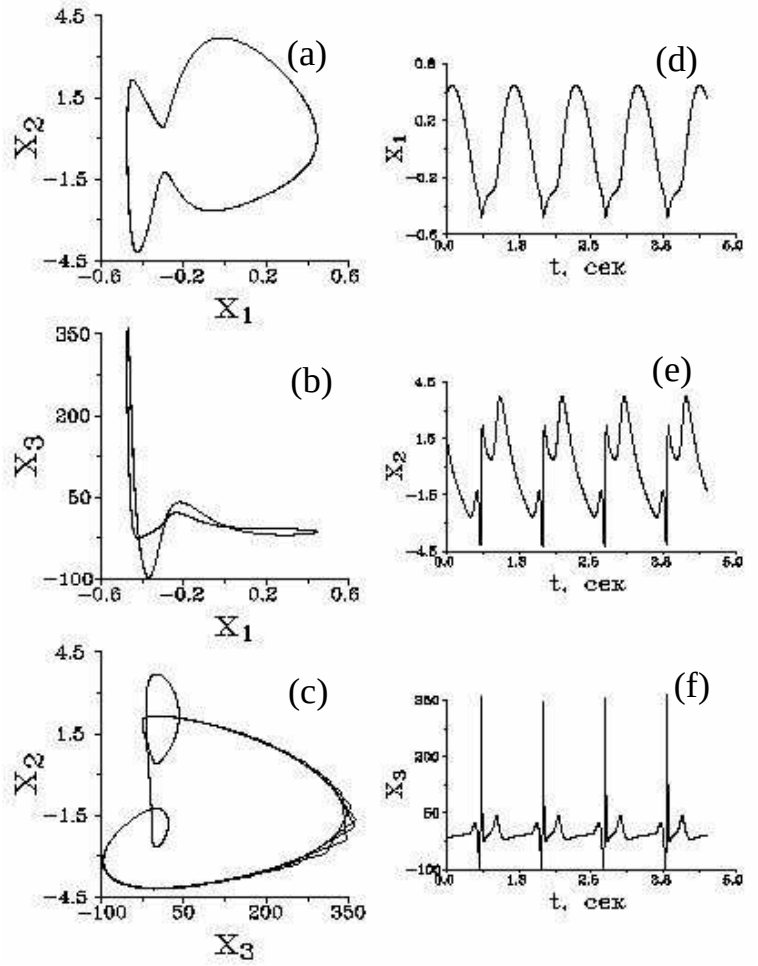

Fig. I.19. (a), (b), (c) Projections of the phase portrait and (d), (e), (f) phase coordinates versus time, of a model reconstructed from phase portrait in Fig. I.18.

An ECG with a slightly different shape was exploited for the second testing of the integration method. The same technique of artificial creation of a periodic signal out of the experimental data was used, and the resulting signal is shown in Fig. I.20(i). Now embedding dimension was chosen to be $N = 4$, and the phase portrait reconstructed by combination of integration and differentiation methods:

$$x_3(t) = a(t),\ x_4(t) = da(t)/dt,\ x_2(t) = \int_0^t x_3(t),\ x_1(t) = \int_0^t x_2(t). \tag{9}$$

The projections of the reconstructed phase portraits and the time dependences of phase coordinates are shown in Fig. I.20. The chosen order of polynomial was $\nu = 3$, and the reconstructed system possessed a periodic solution illustrated by Fig. I.21. The solution of reconstructed systen seems to match the initial data satisfactorily.

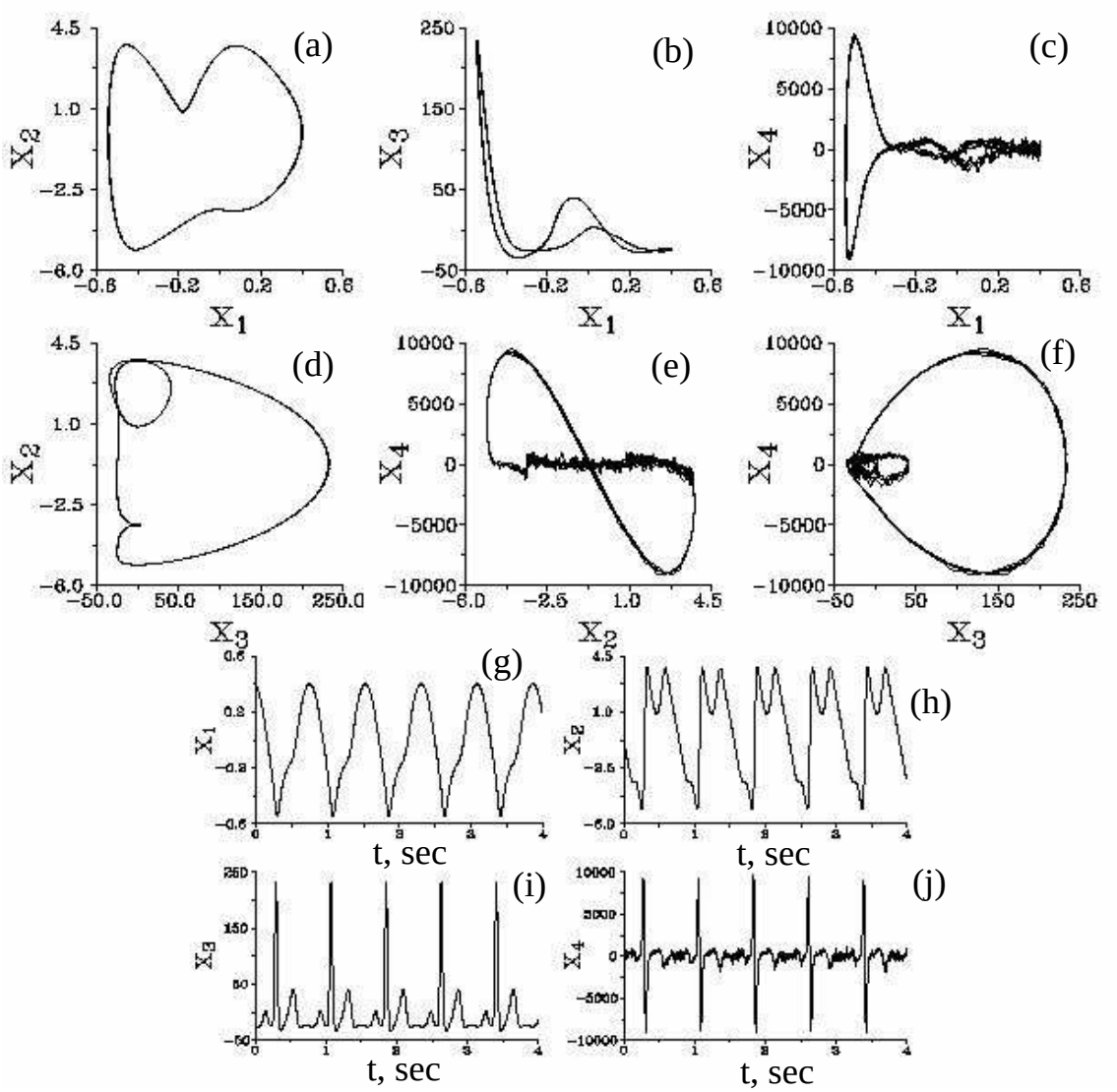

Fig. I.20. (a), (b), (c), (d), (e), (f) Projections of the phase portrait and (g), (h), (i), (j) phase coordinates versus time, reconstructed from ECG by combination of successive integration and derivatives in 4-dimensional phase space. Details are given in text.

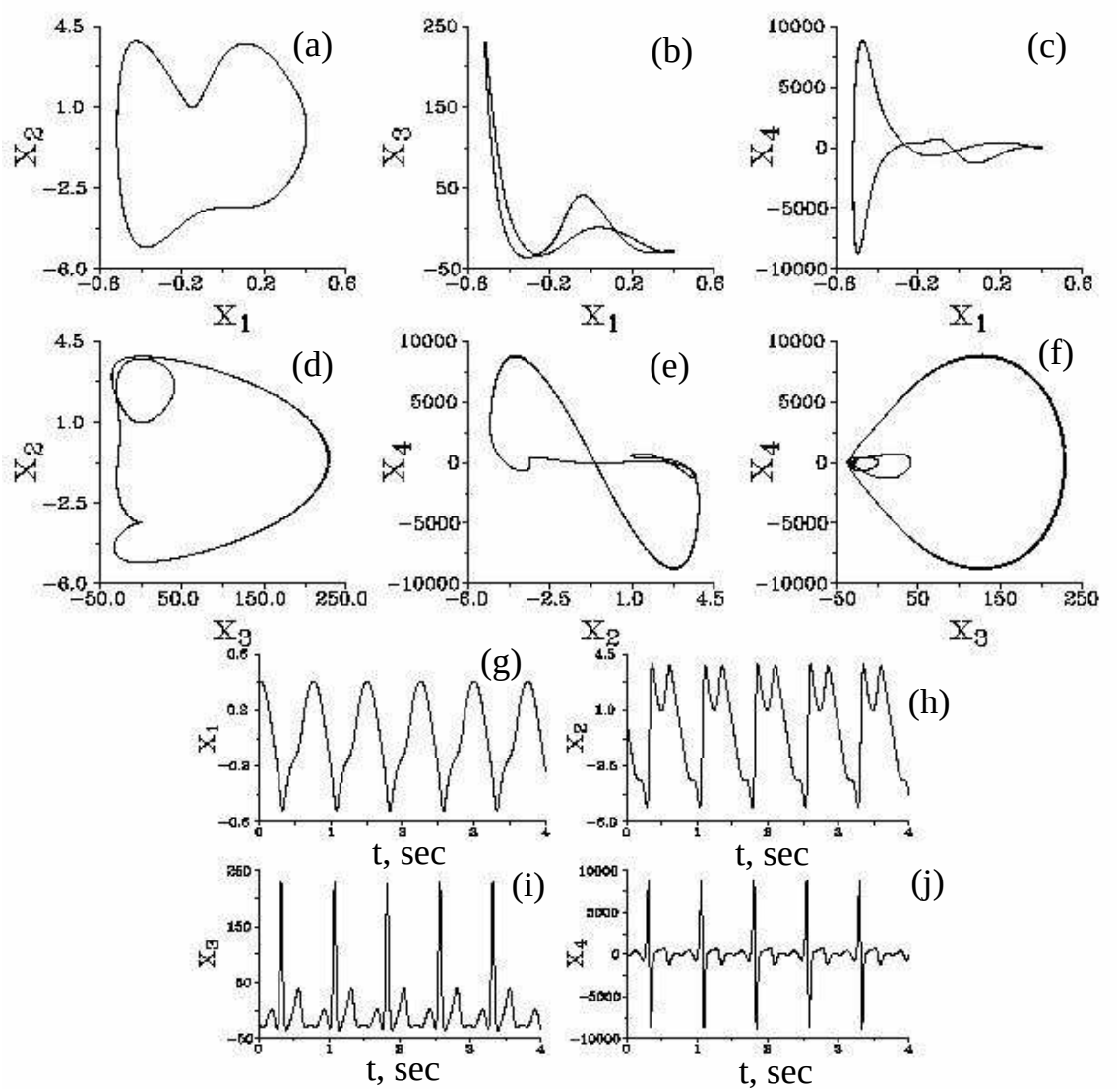

Fig. I. 21. (a), (b), (c), (d), (e), (f) Projections of the phase portrait and (g), (h), (i), (j) phase coordinates versus time, of a model reconstructed from phase portrait in Fig. I.20.

To conclude this section, integration method used for reconstruction of phase portraits from essentially inhomogeneous signals seems to provide a good solution to overcome the problems caused by inhomogeneity of initial data. It leads to the possibility to successfully fit a phase flow with polynomials of moderate orders, and also simplifies the form of the model sought.

II. GLOBAL RECONSTRUCTION IN APPLICATION TO MULTICHANNEL COMMUNICATION

In this Section, we discuss additionally one particular case of the global reconstruction problem. Typically, when processing a scalar time series produced by some system, we do not know even the approximate form of mathematical model that could describe the dynamics under study. Within the framework of reconstruction algorithm, the general form of equations of motion sought is stated *a priori*, e.g., in the following way:

$$\frac{d\vec{x}}{dt} = \vec{F}(\vec{x},\ \vec{\mu^0}); \qquad \vec{x} \in R^n,\ \vec{\mu^0} \in R^k \tag{10}$$

where $\vec{x}$ is the state vector, $\vec{F}$ is the nonlinear vector-function, and $\vec{\mu^0}$ is the parameter vector. In the simplest case, the right-hand parts $F_j(\vec{x},\ \vec{\mu^0}),\ j = 1, \ldots, n$ are defined as a polynomial expansion with a finite number of terms, and the expansion coefficients are fitted numerically. Since there is no possibility to indicate uniquely the *a priori* form of nonlinearities, the task of global reconstruction is related to the class of ill-posed inverse problems. An arbitrary choice of mathematical description is a serious shortcoming of the given technique that results in a variety of problems. In particular, a lot of different equations can be obtained by means of the algorithm discussed in Chapter 1, whose solutions can reproduce the given time series more or less precisely. Also, there is usually no correspondence between the fitted expansion coefficients and the real parameters defining the dynamics of the system under study. The latter means that the set of coefficients restored has no physical interpretation.

The situation changes dramatically if the explicit form of nonlinear functions $\vec{F_j}(\vec{x},\ \vec{\mu^0})$ is known and only the parameter vector $\vec{\mu^0}$ has to be found. Because the main problem vanishes, the problem of reconstruction is not an ill-posed one any longer, and can be solved with the required accuracy. This may lead to various interesting applications. Here we describe one of the possible applications, namely, the problem of multichannel confidential communication.

During the last 10 years, various methods for confidential communication were proposed, based on the idea of using a broadband chaotic oscillations as a carrying (or masking) signal. In most known techniques, in order to extract information signal from the chaotic carrier, the phenomenon of synchronization was applied . In particular, pioneering works in this field [13–18] suggested two major approaches.

The first approach [13–15] uses the notion of synchronization suggested by Pecora and Carroll [19–21]. Within its framework, a chaotic signal $h(t)$ of some oscillator is added to an information message $c(t)$ in the transmitter, i.e., the signal in the channel of communication $s(t)$ represents the sum $s(t) = h(t) + c(t)$. Here, $h(t)$ serves as a masking signal, and its power is much larger than that of $c(t)$. In the receiver consisting of two subsystems, a synchronous chaotic response $h^*(t) = h(t)$ is excited and then subtracted from $s(t)$.

The main idea of the second technique [16–18] consists in the parameter modulation. A control parameter of the chaotic oscillator in the transmitter is modulated according to the binary law. The receiver contains the identical oscillator: when parameters of both oscillators coincide, the synchronous regime is observed, otherwise the dynamics becomes asynchronous.

Further investigations [22–24] extended the possibility of confidential communication using the method of parameter modulation that was previously restricted to the binary code. Moreover, these works solved an important problem of multichannel communication (simultaneous transfer of several messages in a single carrier). When speaking about the multichannel communication, the main question is how to extract information signals from the chaotic background. For this purpose Parlitz et al. [22–24] proposed to apply the *autosynchronization* phenomenon.

All abovementioned approaches require the identity of chaotic oscillators in the receiver and in the transmitter. If they are even slightly non-identical (the difference between parameter values exceeds, e.g., 2%) then the techniques based on the synchronization phenomena are no longer effective [25]. In Refs. [26,27] we suggested an alternative method for confidential communication exploiting the approach of global reconstruction. The ability to extract a single additive influence on the chaotic oscillator by means of the reconstruction was

reported in [28]. By analogy with the works [22–24], we considered a more complex problem: the case of simultaneous transmission of several signals in a chaotic carrier.

The idea of the proposed method is rather simple. Let the carrying signal be generated by a chaotic oscillator described by the mathematical model in the form of Eq. (10) allowing transformation into the form:

$$\frac{dX_1}{dt} = X_2, \quad \frac{dX_2}{dt} = X_3, \quad \ldots, \quad \frac{dX_n}{dt} = f(\vec{X},\ \vec{\mu^0}) \tag{11}$$

by means of variable substitution. (It is indeed possible to realize this transformation for many well-known oscillators such as Chua's circuit, Lorenz and Rössler systems, etc. [29]. Further we shall consider only the oscillators satisfying this requirement.) In order to transmit k messages in a single chaotic signal, the following parameter modulation is implemented:

$$\mu_i^*(t) = \mu_i^0 + \mu_i(t), \qquad i = 1, \ldots, k. \tag{12}$$

Here, μ_i^0 are the fixed values of control parameters, and $\mu_i(t)$ are information signals performing relatively slow modulation, i.e., they are low-frequency in comparison with the carrier. Taking into account Eq. (12), the signal in the communication channel is described by the following nonautonomous equation:

$$\frac{d\vec{x}}{dt} = \vec{F}(\vec{x},\ \vec{\mu}^*(t)). \tag{13}$$

Aiming to solve the task of demodulation (the extraction of transmitted messages), the recipient of information should know the general form of mathematical description Eq. (10). Then he/she is able to uniquely find the current values of control parameters from some fragment of one-dimensional realization $X_1(t)$, which can be measured at the input of the receiver. Because the information signals $\mu_i(t)$ are relatively slow functions of time, it is always possible to choose a temporal window t^* inside which the values of μ_i^* are practically constant, i.e. nonautonomous properties of the system Eq. (13) may not be taken into account. Shifting the temporal window along the carrier, the recipient of information can extract the modulation signals $\mu_i(t)$ almost in real time.

In practice, solving the task of demodulation is implemented as follows. The possibility to rewrite the equations for a chaotic oscillator in the form of Eqs. (11) means that the time dependences of phase variables $X_j(t),\ j = 2, \ldots, n$ can be estimated by numerical differentiation of the carrier $X_1(t)$. Therefore, all left-hand parts and $(n-1)$ of the right-hand parts of Eqs. (11) can be found in each arbitrary instant. As a result, instead of the system of ordinary differential equations we deal with an algebraic (typically linear) equation that generally contains k unknown quantities (the parameter vector $\vec{\mu}^*$). Taking M instants within the limits of temporal window t^* $(M > k)$, the given quantities are easily computed by the least squares technique.

In Ref. [26] as the source of chaotic dynamics we have chosen the Anishchenko-Astakhov oscillator [30] being a rather simple radiophysical model:

$$\begin{aligned} \frac{dx}{dt} &= m_0 x + y - xz, \\ \frac{dy}{dt} &= -x, \\ \frac{dz}{dt} &= -g_0 z + 0.5 g_0 (x + \mid x \mid) x. \end{aligned} \tag{14}$$

By means of variable substitution

$$Y = y, \quad Z = -x, \quad X = -m_0 x - y + xz, \tag{15}$$

the Eqs. (14) are transformed into the following form:

$$\frac{dY}{dt} = Z, \quad \frac{dZ}{dt} = X, \quad \frac{dX}{dt} = f(X, Y, Z, \vec{\mu}), \qquad \vec{\mu} = (m_0, g_0), \tag{16}$$
$$f(X, Y, Z, \vec{\mu}) = \frac{X(X+Y)}{Z} + (m_0 g_0 - 1)Z - g_0(X+Y) + 0.5 g_0(\mid Z \mid -Z)Z^2.$$

If the signal $y(t)$ serves as a carrier, then the dependences $Z(t)$, $X(t)$ and $dX(t)/dt$ can be obtained by numerical differentiation of the time series $y(i\Delta t)$, where Δt is the sampling step. That is why we have only two unknown quantities m_0 and g_0. In order to simplify numerical calculations, suppose that one parameter is fixed ($m_0 = 1.5$) and the function f contains the only unknown quantity g_0. We choose a certain sequence of symbols (letters of the English alphabet) as an information signal. For the purpose of transmission this sequence, split the chosen interval of parameter modulation ($g^*(t) \in [0.2 \div 0.3]$) into 32 subranges each corresponding to some letter or special symbol. Fig. II.1(a) demonstrates an example of information message. The stepwise temporal dependence encoding a word combination *"confidential communication"* is considered as $g^*(t) = g_0 + g(t)$ and each symbol is transmitted during the time related to one step. The carrying chaotic signal of the oscillator described by Eqs. (14) that contains the given message is shown in Fig. II.1(b). The recipient of this signal who knows the explicit form of the mathematical model (16) is able to extract $g^*(t)$ using the reconstruction technique (Fig. II.1(c)).

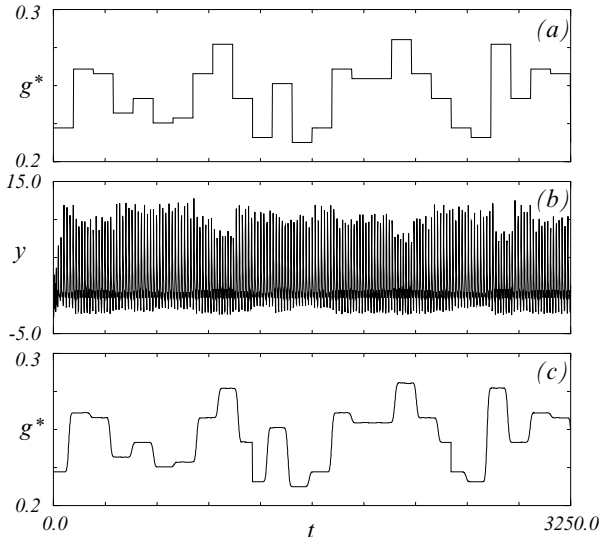

Fig. II.1. (a) an information signal encoding the word combination *"confidential communication"*; (b) the carrying chaotic signal; (c) the restored signal.

Here, we make a few remarks. First, the proposed method for demodulation involves successive differentiation of the carrier. This procedure is obviously accompanied by an increase of numerical errors while estimating each subsequent derivative. These errors can be reduced using various filters. We applied two stages of filtration. Slow parameter modulation allows one to interpret the unknown parameters as constant quantities within the limits of the temporal window t^*. In this case, the least squares technique provides the possibility to obtain some averaged values inside the window (1st stage). When the demodulation is done, any filtration technique can be applied to the extracted signals (2nd stage). All results presented below, that demonstrate the workability of the proposed approach, will be illustrated after the above filtration was applied.

Second, the requirement of slow modulation was introduced. If while making transformations from Eqs.

(14) to Eqs. (16) one needs to compute the derivatives of parameters, this requirement becomes essential. When quick modulation takes place, the function f has more complicated form and includes the terms with dm^*/dt. We have discussed the case of fixed parameter $m^*(t) = m_0 = const$, therefore such terms were absent. If the parameter m_0 is modulated according to the stepwise dependence instead of g_0, the condition of slow modulation is not valid for the moments when $m^*(t)$ switches from one discrete value to another. The latter results in appearance of δ-like peaks related to each switching moment. However, these peaks may easily be filtered out.

Third, when speaking about information transmission, it is necessary to analyze the stability of demodulation with respect to noise. We shall consider the role of various fluctuations below.

Fourth, the algorithm for global reconstruction may be applied to stationary data as well as to time series of transient processes. Indeed, when the values of control parameters are fixed, both the motion on the chaotic attractor and transient processes are described by the same equations. That is why nonstationarity of the carrier is not important when aiming to determine the current values of unknown parameter vector.

By analogy with symbolic sequences, images can be taken for transmission. As an example, Fig. II.2(a) illustrates the Einstein's portrait that was scanned with resolution 500×464 and the obtained data series was used as the encoded message. We have split the range of parameter variation $g^* \in [0.15 \div 0.25]$ into 256 subranges, each corresponding to the shade of the black-and-white image. Information signal performing the parameter modulation has the form similar to Fig. II.1(a). In order to test the used method of demodulation for its robustness, we added white noise with the intensity $D = 10^{-4}$ to $g^*(t)$. Figs. II.2(b) and II.2(c) show the picture in the communication channel and the result of reconstruction, respectively.

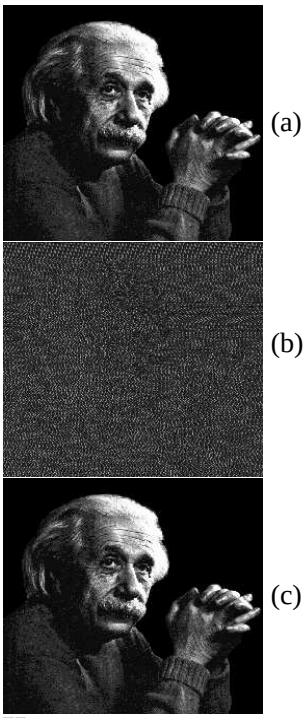

Fig. II.2. (a) the initial portrait; (b) the picture related to the signal in the channel of communication; (c) the restored portrait obtained by means of the global reconstruction technique.

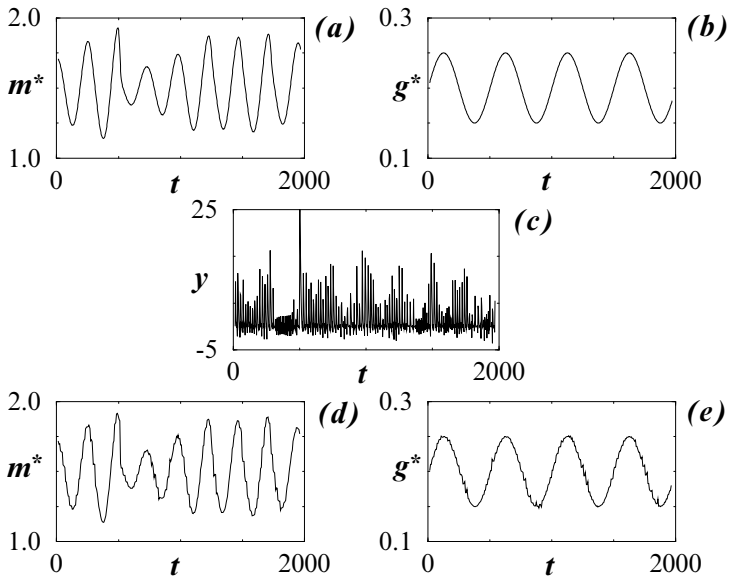

Fig. II.3. (a,b) time dependences of control parameters, (c) the signal in the channel of communication, (d,e) the restored signals.

The next figure demonstrates the possibility of simultaneous transmission of several messages under the noise influence. Parameter m_0 of Eqs. (14) was modulated according to a broadband chaotic signal from the Rössler system and parameter g_0 was changed by the harmonic function as follows:

$$\begin{aligned}
&\frac{dx}{dt} = (m_0 + k_1 x_1 + \xi_1)x + y - xz + \xi_2, \qquad \frac{dy}{dt} = -x, \\
&\frac{dz}{dt} = -g_0(1 + k_2 sin(wt))[z - 0.5(x + \mid x \mid)x],
\end{aligned} \tag{17}$$

$$\frac{dx_1}{dt} = k(-y_1 - z_1), \quad \frac{dy_1}{dt} = k(x_1 + a y_1), \quad \frac{dz_1}{dt} = k(b + z_1(x_1 - c)),$$

where k is the constant parameter that performs the time renormalization to provide a slower process of parameter variation ($m^* = m_0 + k_1 x_1$) compared to the carrier $y(t)$; ξ_1 and ξ_2 are the independent sources of Gaussian white noise each with the intensity 10^{-4}.

Ad-hoc transformation of the Eqs. (17) at the condition of slow modulation allows one to rewrite nonlinear function in the form of Eqs. (16) if the parameters $m^* = m_0 + k_1 x_1$ and $g^* = g_0(1 + k_2 sin(wt))$ are used instead of m_0 and g_0, respectively:

$$f(X, Y, Z, \vec{\mu}) - \frac{X(X+Y)}{Z} + Z = m^* g^* Z - g^*[X + Y + 0.5(\mid Z \mid - Z)Z^2]. \tag{18}$$

Introducing the new quantity $s^* = m^* g^*$, we may consider the Eq. (18) as a linear algebraic equation with 2 unknown parameters s^* and g^*, the latter being estimated from short time series using the least squares technique. Next, if s^* and g^* are found, it is easy to obtain the current value of m^*.

In our study we fix parameters as follows: $k_1 = 0.025$, $g_0 = 0.2$, $m_0 = 1.5$, $w = 0.006$, $k_2 = 0.05$, $k = 0.025$, $a = 0.15$, $b = 0.2$, $c = 10.0$. The temporal dependences of both parameters m^* and g^* are illustrated in Fig. II.3(a,b.) Figs. II.3(d,e) show the results of demodulation that testify to the reliability of the discussed approach in the case of simultaneous transmission of two independent messages in the presence of noise. Now consider another chaotic oscillator being the well-known Lorenz system:

$$\begin{aligned}
&\frac{dx}{dt} = \sigma(y - x), \\
&\frac{dy}{dt} = rx - y - xz, \\
&\frac{dz}{dt} = -bz + xy.
\end{aligned} \tag{19}$$

Here, we choose the coordinate $x(t)$ as the carrying signal. Following the work [29], transformation of Eqs. (19) into the Eqs. (11) leads to the simplest form of nonlinear function f for this coordinate in comparison with the other two variables of Lorenz system. The given transformation is realized using the new variables:

$$X = x, \;\; Y = \sigma(y - x), \;\; Z = \sigma[(r + \sigma)x - (\sigma + 1)y - xz]. \tag{20}$$

As a result, the following system of ordinary differential equations is obtained

$$\begin{aligned}
&\frac{dX}{dt} = Y, \quad \frac{dY}{dt} = Z, \quad \frac{dZ}{dt} = f(X, Y, Z, \vec{\mu}), \qquad \vec{\mu} = (\sigma, r, b), \\
&f(X, Y, Z, \vec{\mu}) = b\sigma(r-1)X - b(\sigma+1)Y - (b + \sigma + 1)Z - X^2 Y - \sigma X^3 + \frac{Y[(\sigma+1)Y + Z]}{X}
\end{aligned} \tag{21}$$

that contains three parameters σ, r and b. Using this model, we shall demonstrate the communication in the case when the parameter b is modulated. The two remaining parameters σ and r will be considered as

constant quantities. Because Y, Z and f can be obtained by the differentiation of time series $x(i\Delta t)$ where Δt is the sampling step (we selected $\Delta t = 0.025$ for all models), b is the single quantity to be found from the last equation. Strictly speaking, for the estimation of the current value of $b(t)$, it is enough to know the phase variables together with their derivatives at a single time instant only. In practice we deal with some temporal window t^* aiming to reduce errors of numerical differentiation.

Fig. II.4 illustrates an example of image transmission. Initial picture (the photo of a building) scanned with the resolution 200×240 is shown in Fig. II.4(a). The range of parameter variation and the signal from the chaotic oscillator under modulation were split into 256 subranges by analogy with Fig. II.2. Fig. II.4(c) demonstrates the result of demodulation.

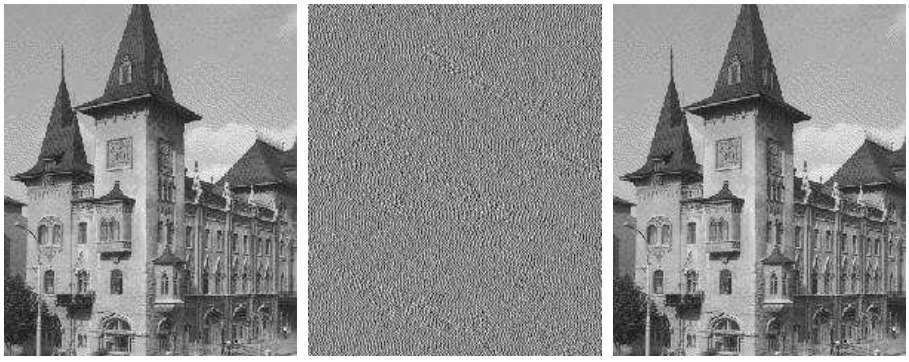

(a) (b) (c)

Fig. II.4. (a) the original photo of a building (the conservatory in the autors' native town Saratov, Russia); (b) the picture related to the signal in the communication channel; (c) the restored photo.

One more example of a chaotic oscillator in our study is Rössler model:

$$\begin{aligned} \frac{dx}{dt} &= -(y+z), \\ \frac{dy}{dt} &= x + ay, \\ \frac{dz}{dt} &= b + z(x-c), \end{aligned} \tag{22}$$

Taking $y(t)$ as the carrier, perform a change of variables:

$$Y = y, \quad Z = x + ay, \quad X = ax + (a^2 - 1)y - z. \tag{23}$$

With the use of new coordinates the equations of Rössler system have the form

$$\frac{dY}{dt} = Z, \quad \frac{dZ}{dt} = X, \quad \frac{dX}{dt} = f(X, Y, Z, \vec{\mu}), \qquad \vec{\mu} = (a, b, c), \tag{24}$$
$$f(X, Y, Z, \vec{\mu}) = -b + (a - c)X - cY + (ac - 1)Z - aY^2 - aZ^2 - aXY + XZ + (a^2 + 1)YZ.$$

With the help of this system we shall demonstrate the simultaneous transmission of three messages in a single carrier. All parameters a, b and c of Eqs. (22) are again modulated for this purpose, e.g., according to the stepwise temporal laws. In such case there is the possibility of transmitting a color image: The modulating signals carry information about the tints of the basic colors (red, blue and green) forming the image. As one can see from Fig. II.5, the applied method of demodulation again demonstrates the efficiency.

Using the Rössler system, we have performed a more detailed investigation of how noise influences the quality of demodulation. We have considered the case when only one parameter (c) is modulated and the remaining

two parameters (a, b) take fixed values. Fig. II.6 illustrates the dependence of the relative error with which the current values of parameter c is determined versus the intensity D of white noise. The latter was added to the parameter c (Fig. II.6(a)), to the first equation of Rössler system (Fig. II.6(b)) and to the carrier (Fig. II.6(c)). Following Fig. II.6, fluctuations in the channel of communication affect the quality of demodulation most severely.

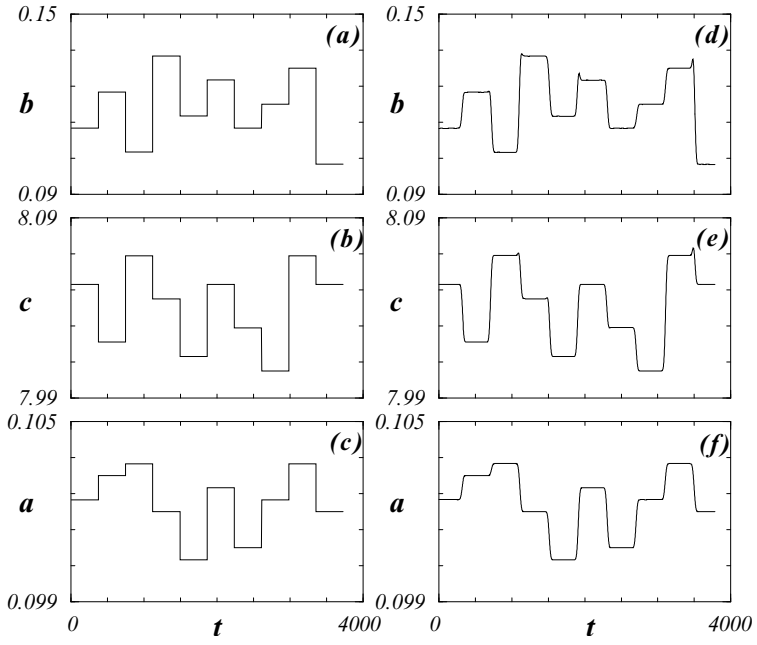

Fig. II.5. (a),(b),(c) - the information signals; (d),(e),(f) - the restored signals.

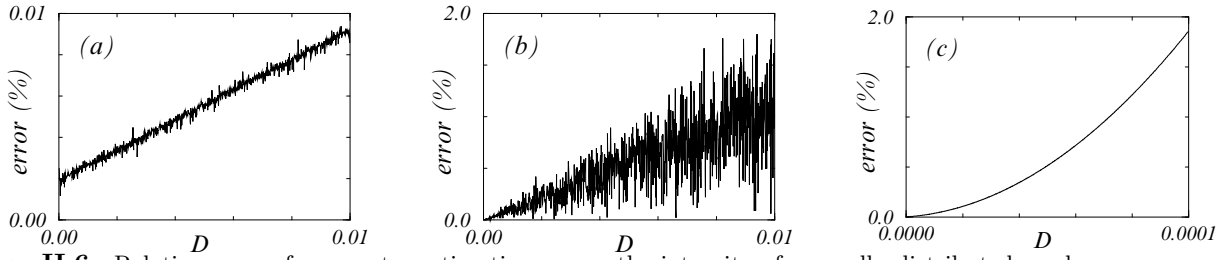

Fig. II.6. Relative error of parameter estimation versus the intensity of normally distributed random process added to the parameter c (a), to the equations (b) and to the carrier (c).

Algorithm parameters like sampling step Δt or the time window t^* are also important quantities. According to Fig. II.7, the value Δt should not be high. At the same time small sampling step also results in an increase of numerical errors.

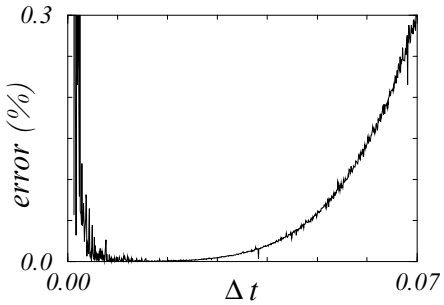

Fig. II.7. Relative error of parameter estimation versus the sampling step for a long enough time series.

To realize the proposed method for signal demodulation in practice, the recipient of information must possess a specialized processor or computer and an analog-to-digital converter. We suppose that such method

for confidential communication may find its application for the exchange of information on short enough distances using cable network, so that noise would not be created while broadcasting.

We have discussed one way for messages encoding that is realized using the parameter modulation. Actually, the global reconstruction technique is not restricted by this approach alone; one can offer its modifications. Let us address the Rössler system again and add some functions of time to the right-hand parts of Eqs. (24):

$$\begin{aligned} \frac{dx}{dt} &= -y - z + A_1(t), \\ \frac{dy}{dt} &= x + ay + A_2(t), \\ \frac{dz}{dt} &= b + z(x - c) + A_3(t). \end{aligned} \tag{25}$$

Suppose that $A_j(t)$ be information signals (they should be slow relative to the carrier $y(t)$). Variable substitutions transforming Eqs. (22) into the form of Eqs. (11) are implemented as follows:

$$Y = y, \quad Z = x + ay + A_2, \quad X = ax + (a^2 - 1)y - z + A_1 + aA_2. \tag{26}$$

$$f(X, Y, Z) = C_1 + C_2 X + C_3 Y + C_4 Z + C_5 XY + C_6 XZ + C_7 YZ + C_8 Y^2 + C_9 Z^2,$$

where

$$\begin{aligned} &C_1 = A_1 A_2 - A_3 + cA_1 - b, \quad C_2 = a - c - A_2, \\ &C_3 = aA_1 - A_2 - c, \quad C_4 = ac + aA_2 - A_1 - 1, \\ &C_5 = C_8 = C_9 = -a, \quad C_6 = 1, \quad C_7 = 1 + a^2 \end{aligned} \tag{27}$$

Unknown quantities C_j are estimated in each instant $i\Delta t$, thereafter the current values of $A_j(t)$ are rather easily calculated from C_2, C_3 and C_1.

Another way for messages encoding may consist in combining the approaches mentioned above: e.g., a part of information signals perform slow parameter modulation and the other part represents the terms added to the right-hand sides of the mathematical model. In particular, let $A_2(t) = 0$, $A_3(t) = 0$ and we would like to transmit 4 messages $a(t)$, $b(t)$, $c(t)$ and $A_1(t)$ simultaneously. Following Eqs. (27) current values of these signals can be estimated from C_j. Thus, a is calculated from $C_5 \div C_9$; c, A_1 and b are obtained from C_2, C_3 and C_1, respectively. Indeed, other combinations could also be considered.

III. ACKNOWLEDGEMENTS

We are grateful to Prof. G.E. Brill from The Central Scientific Laboratory of Saratov Medical University, Russia for giving us signals from the frog heart. Writing of this chapter was supported by Engineering and Physical Sciences Research Council (UK), INTAS (under grant 01-2061) and CRDF (REC-006).

---

[1] F.Takens in *Dynamical Systems and Turbulence*, Warwick, 1980. Vol. 898 of *Lecture Notes in Mathematics*, ed. by D.A. Rang, L.S.Young (Springer, Berlin, 1981) p 366

[2] N.B. Janson, V.S. Anishchenko "Modeling dynamical systems on experimental data", in: Chaotic, fractal, and nonlinear signal processing. AIP Conference proceedings 375. Mystic, CT 1995, pp. 719-725.

[3] N.B. Janson, V.S. Anishchenko "Modeling dynamical systems from experimental data", Izv. VUZ, Applied Nonlinear Dynamics, Vol. 3 (3), 1995, pp. 112-121 (in Russian).
[4] "Physiology", ed. by R.M. Berne, M.N. Levy, Mosby-Year Book (1993).
[5] Anishchenko V.S., Yanson N.B., and Pavlov A.N. "Work of the Human Heart: A Regular Process?", Journal of Communications Technology and Electronics, Vol. 42, No. 8, 1997 pp. 936-940
[6] Anishchenko V.S., Janson N.B. and Pavlov A.N. "Saddle focus in a model of the electrical activity of the human heart", Technical Physics Letters, 22, 168-170 (1996)
[7] Janson N.B., Pavlov A.N., Anishchenko V.S. "One method for restoring inhomogeneous attractors", Int. Journal of Bifurcation and Chaos, 8, 825-833 (1998)
[8] Janson N.B., Pavlov A.N., Balanov A.G. and Anishchenko V.S. "Reconstructing a mathematical model as applied to an electrocardiogram", Technical Physics Letters, 22, 669-671 (1996)
[9] Pavlov A.N., Janson N.B., "Application of Global Reconstruction Technique to Electrocardiogram", Izv. vuz, Applied Nonlinear Dynamics, 5, N 1, pp. 93-108 (1997) (in Russian)
[10] A. Babloyantz, A. Destexhe "Is the normal heart a periodic oscillator?" Biological Cybernetics, Volume 58, Issue 3, 1988, Pages 203-211
[11] Saparin PI, Zaks MA, Kurths J, et al. (1996) Reconstruction and structure of electrocardiogram phase portraits Phys. Rev. E **54** (1), 737-742.
[12] Shil'nikov, L.P., in: Hopf Bifurcation and Its Applications (Applied Mathematical Science Volume 19) by M. McCracken, Jerrold E. Marsden, Springer Verlag (1976).
[13] Kocarev, L., Halle, K.S., Eckert, K., Chua, L.O. and Parlitz, U. (1992). Experimental demonstration of secure communications via chaotic synchronization. Int. J. Bif. Chaos. **2**, 709-713.
[14] Cuomo, K.M. and Oppenheim, A.V. (1993). Circuit implementation of synchronized chaos with applications to communications. Phys. Rev. Lett. **71**, 65-68.
[15] Wu, C.W. and Chua, L.O. (1993). A simple way to synchronize chaotic systems with applications to secure communication systems. Int. J. Bif. Chaos. **3**, 1619-1627.
[16] Parlitz, U., Chua, L.O., Kocarev, L., Halle, K.S. and Shang, A. (1992). Transmission of digital signals by chaotic synchronization. Int. J. Bif. Chaos. **2**, 973-977.
[17] Cuomo, K.M., Oppenheim, A.V. and Strogatz, S.H. (1993). Synchronization of Lorenz-based chaotic circuits with application to communications. IEEE Trans. Circuits Syst. **40**, 626-633.
[18] Dedieu, H., Kennedy, M.P. and Hasler, M. (1993). Chaos shift keying: modulation and demodulation of a chaotic carrier using self-synchronizing Chua's circuit. IEEE Trans. Circuits Syst. **40**, 634-642.
[19] Pecora, L.M. and Carroll, T.L. (1990). Synchronization in chaotic systems. Phys. Rev. Lett. **64**, 821-824.
[20] Pecora, L.M. and Carroll, T.L. (1991). Driving systems with chaotic signals. Phys. Rev. A. **44**, 2374-2383.
[21] Carroll, T.L. and Pecora, L.M. (1991). Synchronizing chaotic circuits. IEEE Trans. Circuits Syst. **38**, 453-456.
[22] Parlitz, U. (1996). Estimating model parameters from time series by autosynchronization. Phys. Rev. Lett. **76**, 1232-1235.
[23] Parlitz, U. and Kocarev, L. (1996). Multichannel communication using autosynchronization. Int. J. Bif. Chaos. **6**, 581-587.
[24] Parlitz, U., Kocarev, L., Stojanovski, T. and Preckel, H. (1996). Encoding messages using chaotic synchronization. Phys. Rev. E. **53**, 4351-4361.
[25] Starkov S.O., Yemetz S.V. (1997). Digital communication systems, using chaos. Proceedings of the 1st International Conference "Control of Oscillations and Chaos", St.Peterburg, August 27-29, 1997, ed. by F.L. Chernousko, A.L. Fradkov, Vol. 2 of 3, pp. 207-210.
[26] Anishchenko, V.S. and Pavlov, A.N. (1998). Global reconstruction in application to multichannel communication. Phys. Rev. E. **57**, 2455-2457.
[27] Anishchenko V.S., Pavlov A.N., Janson N.B. (1998). Global reconstruction in the presence of *a priori* information. Chaos, Solitons and Fractals **9**, 1267-1278.
[28] Gribkov, D.A., Gribkova, V.V., Kuznetsov, Y.I. and Rzhanov, A.G. (1995). Global dynamical modeling of time series and applications to restoration of broadband signal characteristics, in *Chaotic, Fractal and Nonlinear Signal Processing, Mystic, Juli, 1995*, ed. R.A. Katz, (AIP Conf. Proc. **375**, AIP Press, New York), pp. 181-188.
[29] Gouesbet, G.and Letellier, C. (1994). Global vector-field reconstruction by using a multivariate polynomial L_2 approximation on nets. Phys. Rev. E. **49**, 4955-4972.
[30] Anishchenko, V.S. (1995) Dynamical Chaos – Models and Experiments, edited by L. Chua, World Scientific, Singapore. 400 pp.